Short Communication: Ambient Vibration Modal Analysis of Rock Arches using Enhanced Frequency Domain Decomposition and Covariance-driven Stochastic Subspace Identification

Mauro Häusler[1], Paul R. Geimer[2], Riley Finnegan[2], Donat Fäh[1], Jeffrey R. Moore[2]

5   [1]Swiss Seismological Service, ETH Zurich, Zurich, 8092, Switzerland
[2]Department of Geology and Geophysics, University of Utah, Salt Lake City, 84112, USA

Correspondence to: Mauro Häusler (mauro.haeusler@sed.ethz.ch)

Abstract

Natural rock arches are rare and beautiful geologic landforms with important cultural value. As such, their
10   management requires periodic assessment of structural integrity to understand environmental and anthropogenic influences on arch stability. Measurements of passive seismic vibrations represent a rapid and non-invasive technique to describe the dynamic properties of natural arches, including resonant frequencies, modal damping ratios, and mode shapes, which can be monitored over time for structural health assessment. However, commonly applied spectral analysis tools are often limited in their ability to resolve characteristics of closely spaced or complex higher-order modes. Therefore, we investigate two
15   algorithms well-established in the field of civil engineering through application to a set of natural arches previously characterized using conventional seismological techniques. Results from enhanced frequency domain decomposition and parametric covariance-driven stochastic subspace identification modal analyses showed generally good agreement with spectral peak-picking and frequency-dependent polarization analyses. However, we show that these advanced techniques offer the capability to resolve closely spaced modes and provide stable damping estimates. In addition, due to preservation of phase
20   information, enhanced frequency domain decomposition allows for direct and convenient three-dimensional visualization of mode shapes. These advanced techniques provide more detailed characterization of dynamic parameters, which can be monitored to detect structural changes indicating damage and failure, and in addition have the potential to improve numerical models used for arch stability assessment. Results of our study encourage broad adoption and application of these advanced modal analysis techniques for dynamic analysis of a wide range of geological features.

25   # 1 Introduction

Natural arches are rock landforms formed by erosion (Bruthans et al., 2014;Ostanin et al., 2017) and are major tourist attractions worldwide. However, ongoing erosion will eventually lead to partial failure or complete collapse of these landforms, posing a hazard to visitors; prominent recent examples include collapse of London Bridge (Australia) in 1990 (Woodroffe, 2002), rockfall from Landscape Arch (USA) in 1991 and 1995 above a hiking trail (Deseret News, 1991), and collapse of the

30   Azure Window in Malta in 2017 (Satariano and Gauci, 2019). Ambient vibration surveys of arches and other rock features have recently been employed to improve site characterization and hazard assessment associated with failure (e.g., Bottelin et al., 2013;Burjánek et al., 2018;Iannucci et al., 2020;Kleinbrod et al., 2019;Mercerat et al., 2021;Moore et al., 2018). Therefore, passive seismic measurements provide non-invasive means to monitor dynamic behavior and evaluate stability relating to natural or anthropogenic stimuli, which is especially valuable at culturally important sites.

35   The dynamic properties of a structure can be characterized by its natural frequencies, corresponding mode shapes (i.e., structural deflection at those frequencies) and damping ratios (e.g., Chopra, 2015). While damping describes internal energy dissipation and radiation out of the system, resonant frequencies are primarily a function of stiffness and mass. As the mass of a rock landform is approximately constant over time (in the absence of precipitation or mass wasting events), variations in resonant frequencies arise primarily due to changes in rock mass stiffness, which is in turn correlated with rock damage

40   (Colombero et al., 2021). As internal crack growth accumulates during progressive failure, stiffness and thus frequencies are anticipated to decrease; for example, Lévy et al. (2010) reported a drop in resonant frequency of about 20 % less than two weeks prior to collapse of a 21,000 m³ rock column, which they attributed to progressive failure. Therefore, measurements of frequencies over time are potentially valuable for structural health monitoring and early-warning of failure, especially at culturally sensitive sites like rock arches where more invasive monitoring techniques may not be permitted.

45   Currently, simple tools for rock arch stability assessment do not exist. One monitoring approach involves repeated measurements or continuous surveillance of the structure by ambient vibration monitoring and comparing the current resonance attributes (resonant frequency, mode shapes, damping ratio) with an empirical model to detect any deviations from the long-term behavior, which could be interpreted as precursors of failure (e.g., Häusler et al., 2021). For more quantitative assessment, however, individual features need to be numerically modelled. Moore et al. (2020) computed the three-

50   dimensional static stress field for a set of natural rock arches to detect features with high internal tensile stresses, which may be more prone to tensile crack growth and thus failure. However, these models require estimates of rock density and Young's modulus as input parameters, as well as calibration of boundary conditions. While density can be retrieved from rock samples, few observational tools are available to compute the Young's modulus of rock masses and even fewer to calibrate structural boundary conditions. However, these can be estimated using numerical models by minimizing the error between observed and

55   modelled resonance attributes, with the resonant frequency being the dominant contributor (Moore et al., 2018). Therefore, Geimer et al. (2020) performed ambient vibration modal analysis on a large set of natural rock arches, calibrating the material properties and boundary conditions of numerical eigenfrequency models against experimental data which were then used by Moore et al. (2020) for static stress analysis supporting stability assessment.

       Modal analysis techniques used in structural health monitoring of geological features rely primarily on identification

60   of spectral attributes from in-situ ambient vibration data. Power spectra visualizations provide the means for first interpretation, often leading to identification of resonant frequencies that can be confirmed through numerical modeling (Moore et al., 2018), while site-to-reference spectral ratios may be used to eliminate source and path effects and can help to identify and track resonant frequencies (Weber et al., 2018). Frequency-dependent polarization analysis provides a tool to estimate the modal

deflection at resonance (Burjánek et al., 2012;Geimer et al., 2020). However, these basic spectral analysis techniques fall short
when applied to more complex systems, such as cases with closely spaced and overlapping modes that have similar frequencies
but different mode shapes. In addition, phase information is not preserved across separate recording stations, impeding precise
determination of mode shapes for higher modes. Thus, new techniques are necessary to provide refined modal analysis suitable
for structural health monitoring of rock landforms and provide accurate input parameters for stability assessment using
numerical models. Among these, Enhanced Frequency Domain Decomposition (EFDD, Brincker et al., 2001b;Brincker et al.,
2001a) is a promising approach to identify resonant frequencies, damping, and polarization attributes, and is well-suited to
distinguish closely spaced modes. The Covariance-driven Stochastic Subspace Identification (SSI-COV) is an alternative time-
domain technique that is especially beneficial for accurate estimates of modal damping ratios (van Overschee, 1996). Since
their introduction, both techniques have found wide application on engineered structures (e.g., Brincker and Ventura, 2015).
Recently, frequency domain decomposition was applied on natural structures, such as sedimentary valleys, glaciers, and rock
slope instabilities (Poggi et al., 2015;Preiswerk et al., 2019;Häusler et al., 2021), while the application of SSI-COV remained
restricted to artificial structures.

In this study, we focus on four natural rock arches in Utah (USA), previously investigated by Geimer et al. (2020)
and Moore et al. (2020). As these arches exhibit various spectral complexities that complicate interpretation, we apply two
operational modal analysis techniques - EFDD and SSI-COV - to improve identification and characterization of normal modes.
The strengths of these techniques lie in the analysis of closely spaced and hidden modes, and in the preservation of phase
information between different components, allowing for the direct retrieval of mode shape information at each sensor location.
Our results highlight the value and versatility of EFDD and SSI-COV techniques for structural health monitoring and geologic
hazard applications, which we propose is useful in a broad range of natural features beyond our studied landforms, for example,
rock slope instabilities and freestanding rock towers.

2 Methods

Ambient vibration data processed in this study were collected at four natural rock arches in Utah by Geimer et al.
(2020). These consist of three single-station measurements conducted using a Nanometrics Trillium Compact 20-s
seismometer (sites: Rainbow Bridge, Corona Arch, Squint Arch) and two array measurements using three-component Fairfield
Zland 5-Hz nodal geophones (sites: Squint Arch and Musselman Arch). Table 1 summarizes the arch measurements, including
data acquisition length, site coordinates, and number of sensors deployed. Prior to processing, all data were corrected using
the respective instrument response (to velocity units of m/s), and the mean and linear trend were removed.

Table 1: Location, span, and data acquisition characteristics for each arch investigated (coordinates in WGS84, date-time in UTC).

Site	Span [m]	Latitude	Longitude	Number of sensors	Acquisition date	Duration
Rainbow Bridge	84	37.07748	-110.96415	1	24 March 2015	3 hours
Corona Arch	34	38.57997	-109.62008	1	8 October 2017	1 hour
Squint Arch	12	38.64651	-110.67388	1 6	1 February 2018 30 April 2018	1 hour 2 hours, 50 minutes
Musselman Arch	37	38.4359	-109.76987	32, arranged in two parallel lines	14 February 2017	2 hours

95

We processed three-component ambient vibration data using Enhanced Frequency Domain Decomposition (EFDD), which is an output-only modal analysis technique used in civil engineering (Brincker et al., 2001b;Brincker et al., 2001a;Brincker and Ventura, 2015;Michel et al., 2010). The method first computes the cross-power spectral density between all input traces and for every discrete frequency. Next, singular value decomposition for each frequency provides the singular
100   values and singular vectors. The first singular value shows peaks at the dominant natural frequencies of the system, with peaks on higher singular values indicating overlapping secondary (i.e., non-dominant) modes. Resonant frequencies are then determined from analysis of the singular value plot, and the singular vector at the identified frequencies gives the three-dimensional modal vector (i.e., shape) of the chosen mode.

In order to estimate modal damping, the mode bell of each resonant frequency is picked manually and transformed to
105   the time domain, providing the impulse response function. Energy decay in the linear part of the impulse response function is expressed by the damping ratio ζ, which can be determined using the logarithmic decrement technique (Cole, 1973). Linear regression of the zero-crossing times within the linear part of the decay curve additionally provides an updated estimate of the resonant frequency. Detailed description of the EFDD processing workflow applied in this study can be found in Häusler et al. (2019) and Häusler et al. (2021), which applied the algorithm to unstable rock slopes.
110   The second technique used in this study is the Covariance-driven Stochastic Subspace Identification (SSI-COV) method (van Overschee, 1996;Peeters and De Roeck, 1999). Like EFDD, SSI-COV is an output-only technique used in civil engineering. Contrary to EFDD, SSI-COV is a time-domain parametric technique, which searches for the best set of modal parameters (resonant frequencies and modal damping) representing the observed structural response in a least-square sense, i.e., minimizing the sum of squares of the residuals between model and observed data. The most important parameter is the
115   maximum lag time between two time samples used for computing the covariance matrices, which should be two to six times larger than the longest eigenperiod of the structure. Other user-controlled parameters include the number of possible modes (i.e., poles), the accuracy threshold for modal frequency variations, the minimum spectral distance between two adjacent modes, and the variation of the minimum modal assurance criterion (e.g., Allemang and Brown, 1982), which is a measure of the similarity of the mode shape at neighbouring frequencies. Parameter combinations for every arch can be found in Table A1
120   in the appendix. Since SSI-COV is a parametric method, its resulting resonant frequencies should be verified by a frequency-

domain technique to prevent misinterpretation by model overfitting. We applied the SSI-COV algorithm by Cheynet (2020), which is based on the implementation by Magalhães et al. (2009) and was used for comparison to EFDD on long suspension bridges (Cheynet et al., 2017). Using these same complementary techniques, Bayraktar et al. (2015) found a good agreement between EFDD and SSI-COV in their study on historical masonry arch bridges with resonant frequencies and damping ratios

125   comparable to the natural rock arches and bridges studied here.

Results from SSI-COV (and other SSI variants) are illustrated using stability diagrams (e.g., Figure 1c). Initially, the structure's response is modelled with a low number of modes (poles), which is continuously increased to the maximum number of poles defined by the user. The resulting resonant frequencies for each mode at every model run are plotted in the stability diagram (blue crosses in Figure 1c). Repeated poles, i.e., identical or very similar values for resonant frequencies, damping,

130   and mode shape, represent stable poles and can be identified as vertical stacks of poles in the stability diagram (red circles in Figure 1c). Poles not fulfilling the user-defined accuracy criteria are not interpreted as stable poles and are scattered at arbitrary values as a result of noise fitting. Stable poles are clustered using hierarchical clustering, grouping poles with similar characteristics to the final resonant modes of the structure.

3 Results

135   We observe the first three resonant modes of Rainbow Bridge at 1.1, 2.2, and 2.5 Hz (Figure 1a-c). While the fundamental mode (f_1 at 1.1 Hz) is distinctly separated from other spectral peaks, the second and third modes (f_2, f_3) occur at closely spaced frequencies but are clearly identified by the elevated second singular value. Damping is between 0.6 and 1.3 % for all three modes (Table 1). For the fundamental mode, we estimate damping at 0.9 and 0.6 % using EFDD and SSI-COV, respectively, which is significantly lower than estimated by Geimer et al. (2020) using the half-power bandwidth method

140   (2.4 %). Modal vectors (i.e., azimuth and incidence angle with a lower hemisphere projection) derived by EFDD are very similar to the polarization analysis (PA) of Geimer et al. (2020) with some minor differences for f_3 and a 180° ambiguity in the azimuth of the nearly horizontally polarized mode f_2. Note that Geimer et al. (2020) allowed a polarity flip for mode shapes with sub-horizontal incidence angles equal to or larger than 85° in order to compare to numerical models. As SSI-COV and EFDD provide similar results, we only compare values from EFDD to PA in Table 2 and provide SSI-COV results in Table A2

145   in the appendix.

Earth **Surface**
Dynamics
Discussions
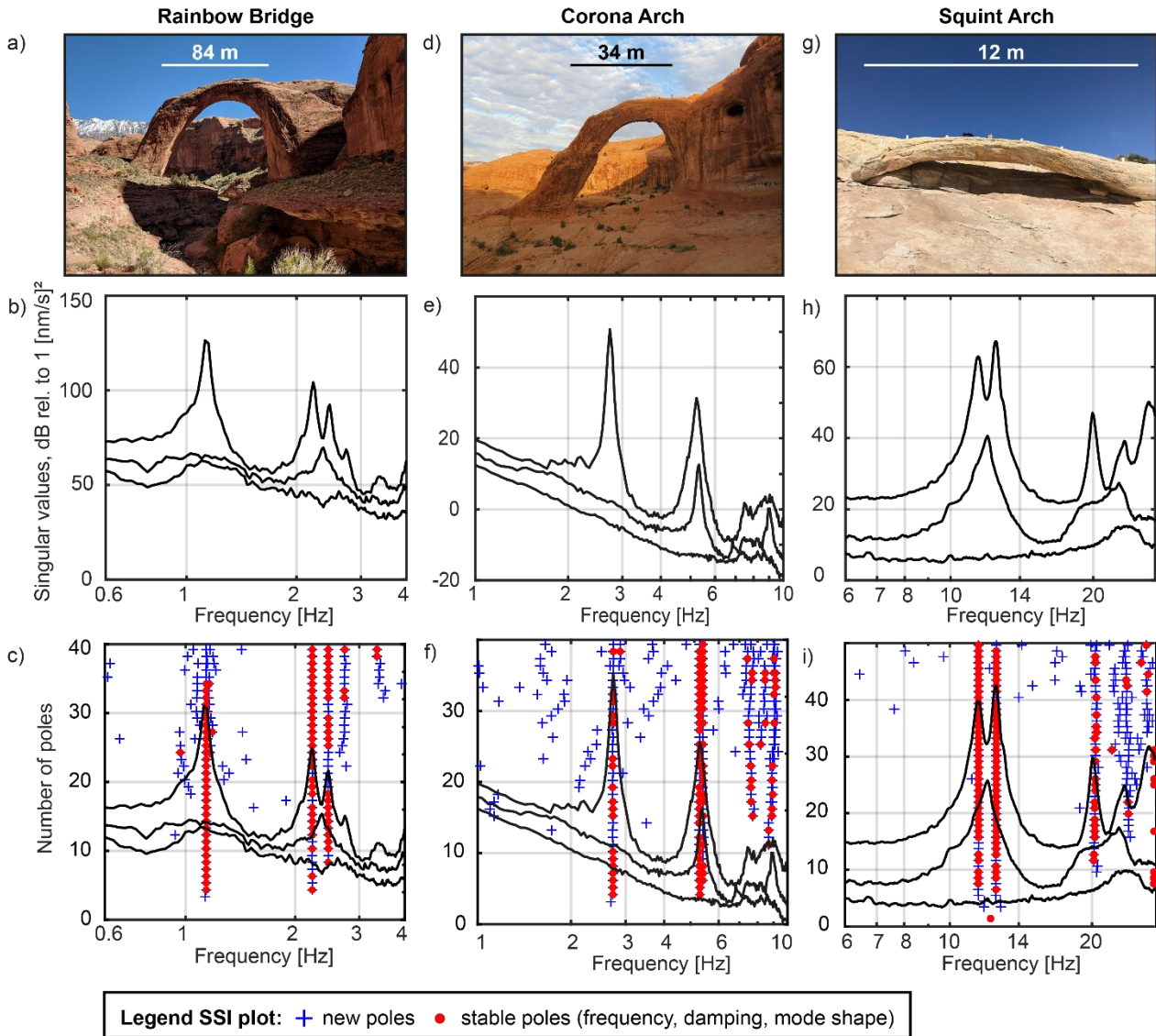
Figure 2: a) Photograph of Rainbow Bridge, b) singular value plot of EFDD analysis at Rainbow Bridge, c) singular value plot of Rainbow Bridge with SSI-COV poles superimposed with increasing number of poles. Each pole is marked with a blue cross, stable poles (in terms of resonant frequency, mode shape, and damping ratio) are marked with a red circle. Unstable poles (i.e. blue crosses at distance from stable poles) arise from noise fitting. Subplots d) to f) and g) to i) are the same as a) to c) for Corona Arch and Squint Arch, respectively. Photographs in panels a) and d) from Moore et al. (2020).

The singular value plot of Corona Arch reveals two distinct spectral peaks at 2.7 and 5.3 Hz (Figure 1d-f). However, the second singular value also peaks at ~5.3 Hz, indicating the presence of a closely spaced mode at that frequency. Therefore, we confirm the interpretation of two close modes by Geimer et al. (2020). However, EFDD and SSI-COV suggest nearly identical frequencies for f_2 and f_3 (5.3 Hz) while Geimer et al. (2020) selected more separated frequencies (5.0 and 5.4 Hz) based on PA. Modal vectors for f_1 and f_2 resolved by PA and EFDD are in good agreement, however azimuth and incidence

differ for f_3. While EFDD and SSI-COV gave similar values for modal incidence of f_3 (44° and 54°, respectively), PA estimated incidence at 73°. Damping is estimated between 0.9 and 2.0 % for all three modes, with 0.9 and 1.4 % for the fundamental

160   mode (via SSI-COV and EFDD, respectively). These values are again slightly lower than the half-power bandwidth estimates of Geimer et al. (2020, 1.9 %). Damping ratios for f_2 and f_3 are between 1.5 and 2.0 % with good agreement between EFDD and SSI-COV.

For Squint Arch, we observe two closely spaced modes at 11.5 and 12.5 Hz, and a third mode at 19.9 Hz (Figure 1g-i). The second mode was not analysed by Geimer et al. (2020) as it could not be confirmed as a separate mode by numerical

165   models. A mode splitting phenomenon, for example, caused by anisotropy, might be a potential explanation for the inability to replicate this mode in homogeneous numerical models. Our analysis of the second mode suggests the modal vector has a steeper incidence angle of 49°, and is therefore oriented 60° from f_1. If the two spectral peaks were analysed separately by PA, the match between PA and EFDD is very good (see values in brackets in Table 2). Geimer et al. (2020) determined modal damping by applying the logarithmic decrement technique to a series of decaying time-series responses created by an active-

170   source impulsive impact. The resulting damping ratio of 1.6 % is in perfect agreement with the estimation by SSI-COV but differs slightly from the EFDD output (2.4 %).

Table 2: Overview of resonant frequencies, modal damping ratios derived by EFDD and SSI-COV, and modal vectors (azimuth and
175 **incidence angle) estimated by EFDD and polarization analysis (PA) for Rainbow Bridge, Corona Arch, and Squint Arch. The**
number in brackets for Squint Arch are the values derived by PA if f_1 and f_2 were interpreted as separate modes (see supplementary
information to Geimer et al., 2020). Incidence angle corresponds to the lower hemisphere projection.

	Frequency [Hz]	Damping EFDD [%]	Damping SSI-COV [%]	Azimuth EFDD [°]	Azimuth PA [°]	Incidence EFDD [°]	Incidence PA [°]
Rainbow Bridge							
Mode f_1	1.1	0.9	0.6	145	145	85	85
Mode f_2	2.2	1.2	0.9	122	304	85	84
Mode f_3	2.5	1.2	1.3	17	23	86	82
Corona Arch							
Mode f_1	2.7	1.4	0.9	70	70	89	89
Mode f_2	5.3	1.9	2.0	248	250	85	83
Mode f_3	5.3	1.5	1.9	225	238	44	73
Squint Arch							
Mode f_1	11.5	2.4	1.6	39	221 (39)	71	61 (72)
Mode f_2	12.5	1.6	1.1	221	n/a (221)	49	n/a (49)
Mode f_3	19.9	1.5	2.0	140	148	16	16

We compare damping ratios estimated by the various techniques for each arch in Figure 2. The resonant frequency
180 and damping ratio derived by each technique are used to model a single-degree-of-freedom (SDOF) system, which is
superimposed on the singular value plots. The amplitude of the modelled SDOF is normalized to the maximum amplitude of
the first singular value. The mode bell of the fundamental mode of Rainbow Bridge is well reproduced by EFDD and SSI-
COV, but damping is overestimated by the half-power bandwidth technique. However, neither SSI-COV nor EFDD is able to
perfectly reproduce the mode bell due to its slightly asymmetric shape, likely reflecting the oversimplified assumption of a
185 SDOF system. SSI-COV and EFDD perform equally well reproducing the mode bells of f_2 and f_3. At Corona Arch, only SSI-
COV is capable of reliably reproducing the mode bell of the fundamental mode, and the half-power bandwidth again
overestimates damping. The second and third mode are well reproduced by both SSI-COV and EFDD. SSI-COV and the
active-source impact test yielded identical damping ratios for the fundamental mode of Squint Arch. However, as for Rainbow
Bridge, a similar match could not be obtained for f_1 and f_2 by any of the techniques. For f_3, EFDD produces a slightly better
190 match with the singular values, while SSI-COV appears to marginally overestimate damping.
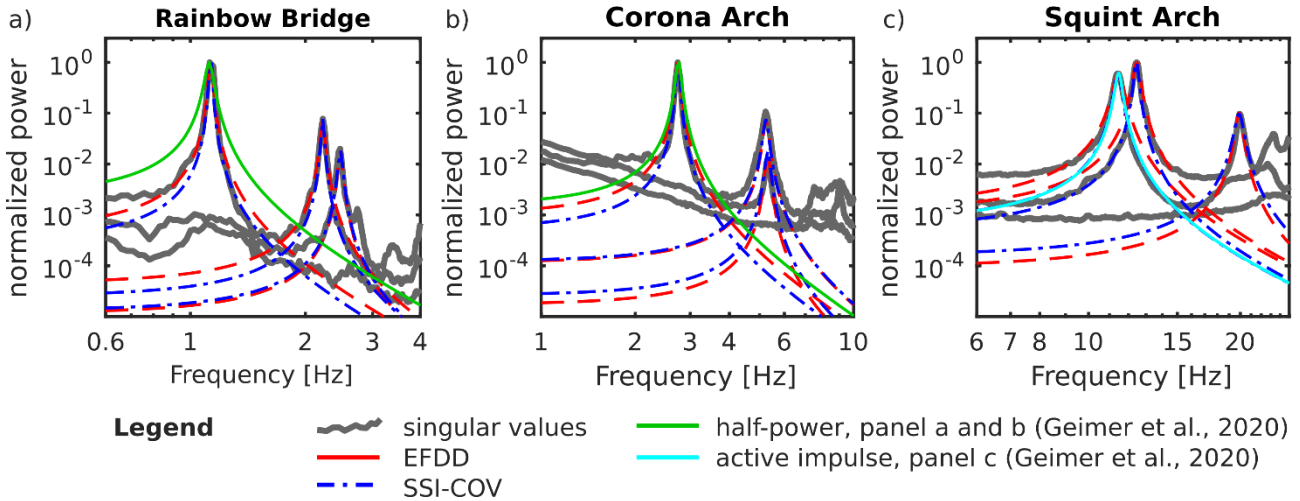
Figure 2: Singular value plots with spectra of single-degree-of-freedom systems modelled by using input data from EFDD (red), SSI-COV (blue), half-power bandwidth technique (green), and active impact measurements (cyan).

The first two modes of Squint Arch can also be resolved from EFDD analysis of data acquired by a nodal geophone
195   array during a separate experiment (Figure 3b) with sufficient station density to extract the full mode shapes. We note that
modal frequencies for f_1 and f_2 increased by about 1 Hz compared to the single-station measurement, which we attribute to
seasonal variations in the dynamic response due to temperature effects (11.5°C for the single-station and 16°C for the nodal
measurement, respectively, see also Starr et al., 2015). No other higher modes are visible on the singular value plot, either
because the noise level of the nodal geophones is too high or because the modes were not excited during the survey. Modal
200   vectors for the first two modes at all stations resulting from EFDD analysis are shown in Figure 3c. We were not able to define
a set of SSI-COV parameters that could successfully reproduce the observed modes, possibly owing to the low excitation level
at the small arch combined with the higher instrument noise level of the nodal geophones compared to the broadband
instruments used in the single-station measurements.

205
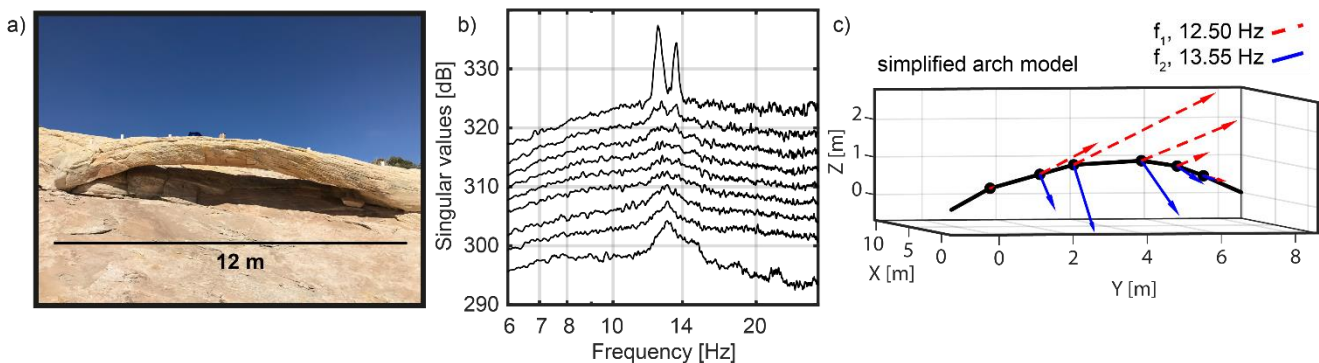
Figure 3: a) Photograph of Squint Arch during the array measurements using nodal geophones, b) singular value plot of EFDD analysis showing the first nine singular values, c) Modal vectors at 12.5 Hz and 13.6 Hz.

We performed EFDD and SSI-COV modal analyses on geophone array data acquired at Musselman Arch revealing the first four resonant modes at 3.4, 4.2, 5.6, and 6.6 Hz (Figure 4b, c). The resonant frequencies and mode shapes are in good

210   agreement with results of the single-component cross-correlation analysis by Geimer et al. (2020). Visualization of the three-dimensional modal vectors for each station determined by EFDD are shown in Figure 4d-g. The first two modes are full-span, first-order bending modes in the horizontal and vertical directions, respectively. The third mode is a near symmetric second-order vertical bending mode with its node point at the centre of the arch. Mode four is a slightly asymmetric second-order horizontal bending mode with the node point shifted towards the eastern abutment. Modal damping ratios for Musselman Arch

215   are estimated to be between 1.3 % and 1.9 %, with EFDD and SSI-COV providing similar results (Table A2 in the appendix).

Earth **Surface**
Dynamics Open Access
Discussions
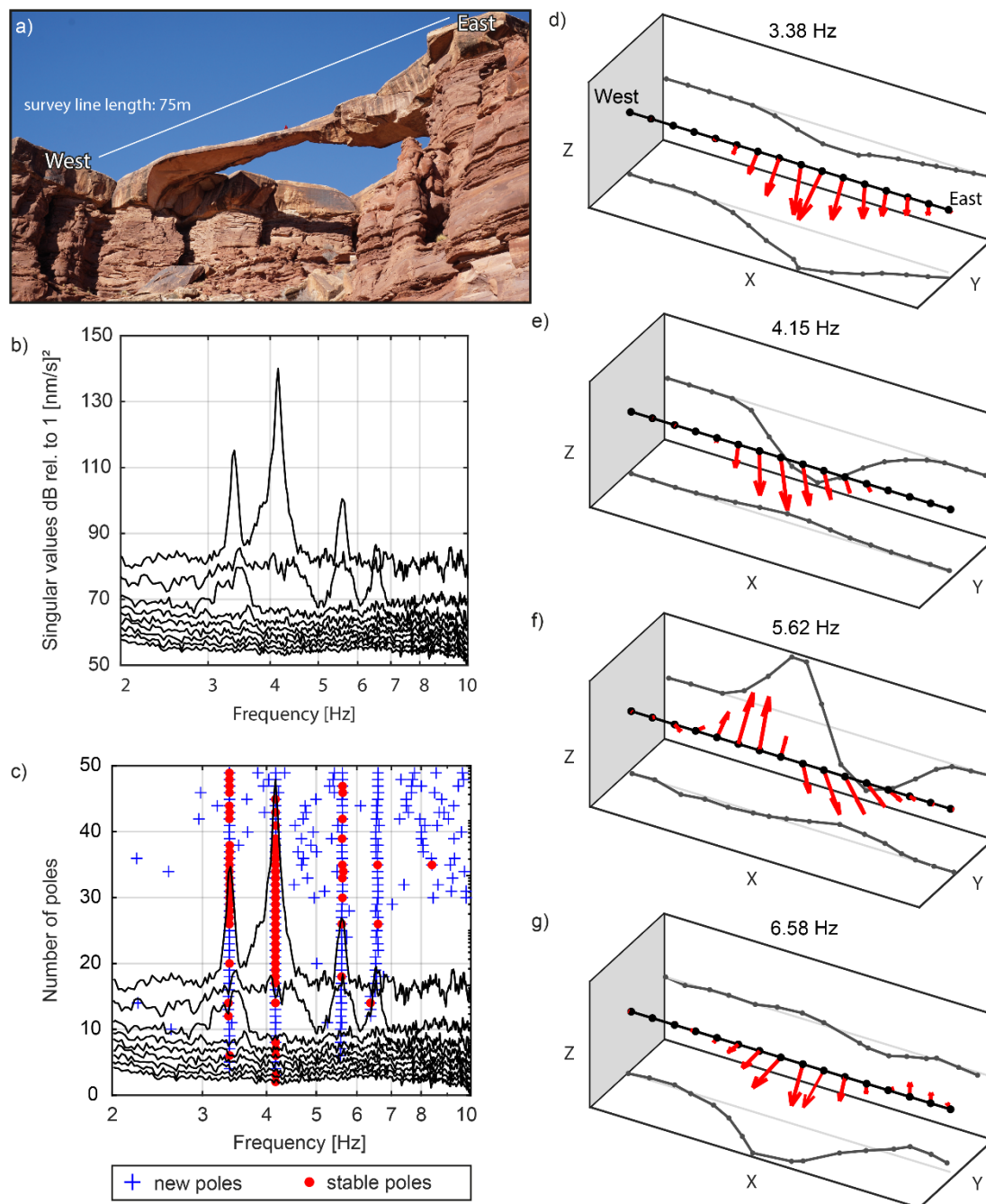
Figure 4: a) Photograph of Musselman Arch, b) first nine singular values of the EFDD analysis, c) singular value plot with SSI-COV poles superimposed: stable frequency (blue cross) and stable mode shape (red circle). d) to g): 3D normal mode shapes at the first four resonant frequencies (3.38 Hz, 4.15 Hz, 5.62 Hz, and 6.58 Hz) with projections onto the X-Z and X-Y planes. For better visibility, only one of the two parallel geophone lines is displayed, while the mode shapes of both lines are comparable (see appendix Figure A1). Photograph panel a) by Kathryn Vollinger.

220

4 Discussion and Conclusions

We applied Enhanced Frequency Domain Decomposition (EFDD) and Covariance-driven Stochastic Subspace
225 Identification (SSI-COV) modal analyses on four natural rock arches that were previously analysed by Geimer et al. (2020)
using frequency-dependent polarization analysis (PA). Our results show that EFDD and SSI-COV are well suited to determine
the natural frequencies, damping ratios, and mode shapes of these geological structures. For clear resonant modes, these
techniques reproduce the results by Geimer et al. (2020). In case of more complex spectra, EFDD and SSI-COV are able to
extract additional modal details not resolved with PA. EFDD facilitated identification and interpretation of closely spaced (i.e.,
230 spectrally overlapping) and hidden modes at Corona and Squint arches. EFDD additionally combines information for all input
traces in a single plot, allowing for a user-friendly analysis of the dynamic response. The singular vectors resulting from EFDD
can be directly interpreted as the three-dimensional modal deflection vector at each station, providing rapid and convenient
visualization of normal mode shapes.

Modal damping estimation from both SSI-COV and EFDD are not based on individual picks on the power spectra,
235 as it is the case for the half-power bandwidth technique. EFDD damping evaluation is based on the shape of the entire mode
bell in the frequency domain, while SSI-COV is a parametric time-domain technique. Therefore, modal damping determined
by these techniques is expected to be more robust than the half-power bandwidth picking technique, which is highly sensitive
to spectral smoothing, resulting in over-estimates of damping at Rainbow Bridge and Corona Arch. This is supported by good
agreement between EFDD, SSI-COV results and damping determined for the active impulse measurement at Squint Arch.
240 However, SSI-COV results are likely to be closer to the physical damping ratio than EFDD, as limitations in spectral resolution
can lead to a broadening of the normal mode bell, and thus overestimation of modal damping determined in the frequency
domain. While EFDD performed well in all cases studied here, SSI-COV failed in one instance using nodal geophones, likely
as a result of low signal to noise ratios and suggesting a possible limitation of the technique or instrumentation requirement
for dynamic analysis of geological features with low ambient excitation.

245 While modal analysis via peak-picking and subsequent PA has been shown to be satisfactory for adequately spaced
spectral peaks and strongly amplified resonant frequencies, here we demonstrate that more sophisticated modal analysis
techniques increase the robustness of the results, especially for more complex dynamic systems, providing refined modal
characterization. Improving the accuracy and our understanding of resonance properties helps generate more refined numerical
models, which can in turn lead to more accurate rock arch stability assessment. Future efforts in modelling the dynamic
250 response of rock arches (and other geological structures) should additionally involve calibration of the modal damping ratio,
as we have shown this parameter can be reliably measured. In addition, we recommend integrating material anisotropy in
numerical models for rock arches exhibiting a complex dynamic response with closely spaced or split modes that could not be
replicated using homogeneous models.

Our results encourage adaptation and widespread application of EFDD and SSI-COV modal analysis techniques,
255 which are commonly used in civil engineering, and complement existing seismological techniques for dynamic analysis of

geological features. Both techniques might be well-suited for future near real-time monitoring of the structural integrity of geological features beyond rock arches, for example, rock slope instabilities, unstable glaciers, and freestanding rock towers.

Appendix A

260 **Table A1: SSI-COV input parameters as defined by Cheynet (2020). Ts: time lag for covariance calculation, Nmin: minimal number of model order, Nmax: maximum number of model order, ε cluster: maximal distance inside each cluster. Frequency accuracy (ε frequency), MAC accuracy (ε MAC) and damping accuracy (ε zeta) are set to 0.01, 0.05 and 0.04 for all analyses, respectively.**

Structure	Ts [s]	Nmin	Nmax	ε cluster	Pass band [Hz]
Rainbow Bridge	2.8	2	40	0.1	0.5 to 6
Corona Arch	1.2	2	40	0.15	0.8 to 12
Squint Arch	0.2	2	60	0.1	4 to 40
Musselman Arch	1.1	2	50	0.5	1 to 20

Table A2: Modal parameters obtained by SSI-COV. Azimuth values labelled with an asterisk (*) show a 180° ambiguity compared
265 **to EFDD and polarization analysis.**

	Frequency [Hz]	Damping [%]	Azimuth [°]	Incidence [°]
Rainbow Bridge				
Mode f_1	1.1	0.6	145	85
Mode f_2	2.2	0.9	122	84
Mode f_3	2.5	1.3	197*	86
Corona Arch				
Mode f_1	2.7	0.9	69	90
Mode f_2	5.2	2.0	72*	87
Mode f_3	5.3	1.9	43*	54
Squint Arch				
Mode f_1	11.4	1.6	219*	71
Mode f_2	12.4	1.1	40*	48
Mode f_3	19.9	2.0	143	16
Musselman Arch				
Mode f_1	3.4	1.3	n/a	n/a
Mode f_2	4.2	1.1	n/a	n/a
Mode f_3	5.6	1.6	n/a	n/a
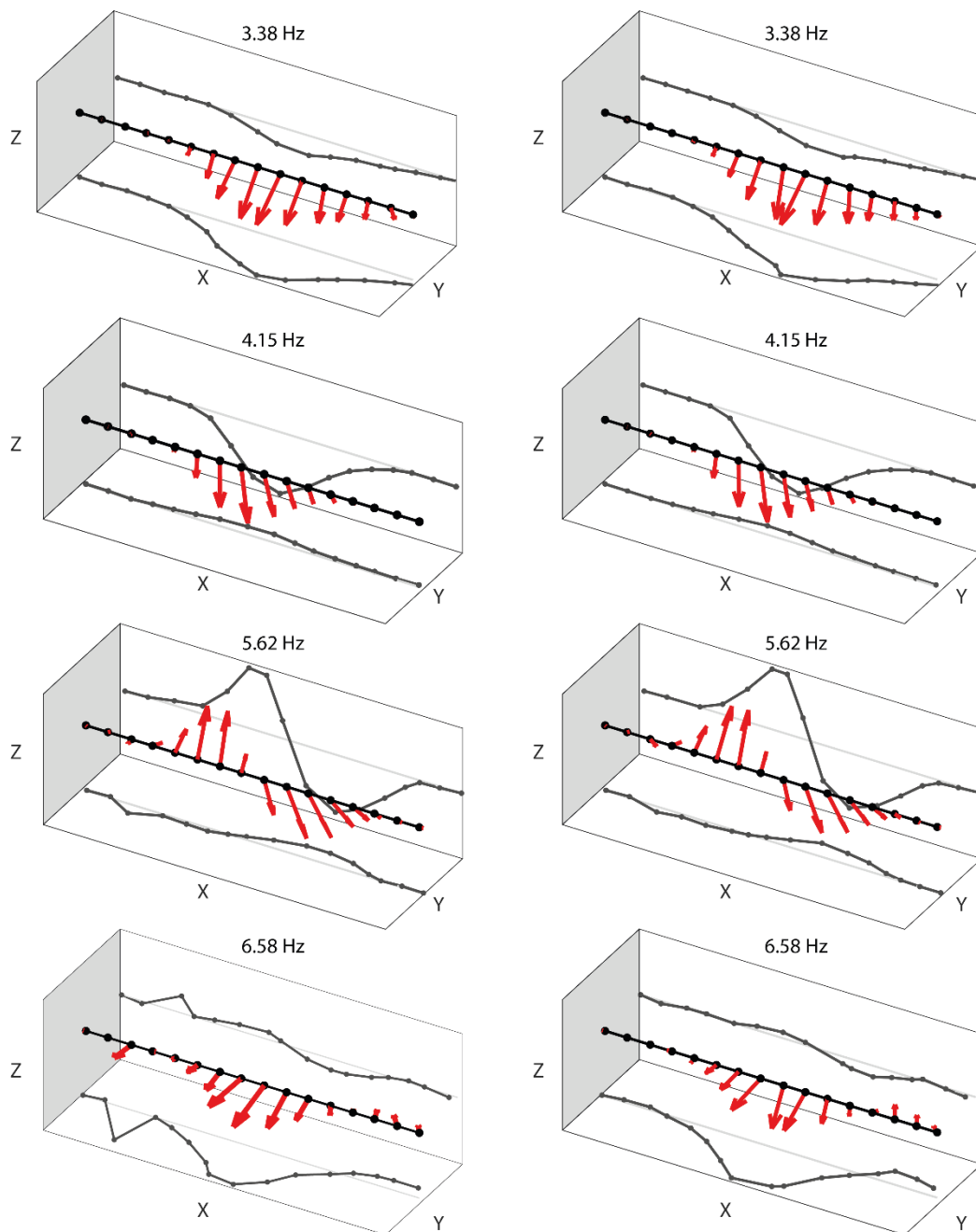
Figure A1: 3D mode shapes of Musselman Arch for the two parallel lines of geophones and projections onto the X-Y and X-Z planes. The geophone line shown on the right is shown in Figure 4d-g in the main article. The mode shapes of the parallel line are nearly identical.

270

Data availability

Data used in this study and originating from the study by Geimer et al. (2020) are available at doi.org/doi:10.7278/S50D-G31E-NFW2. Data of the nodal deployment at Squint Arch are available at https://doi.org/10.7914/SN/5P_2013.

Author contribution statement

275   The manuscript was written by MH with significant contributions from all co-authors. PG, RF, and JM acquired seismic data. MH carried out data processing and software development of EFDD modal analysis. PG performed data curation and validation of results. All authors reviewed and approved the manuscript.

Competing interests

The authors declare that they have no conflict of interest.

280   **Acknowledgements**

Support for this study was provided by the US National Science Foundation Grant EAR-1424896. M. Häusler was financed by ETH project grant 0-20361-17.

References

Allemang, R. J., and Brown, D. L.: A Correlation Coefficient for Modal Vector Analysis, 1st International Modal Analysis Conference
285   (IMAC I), Orlando, 1982, 110-116,

Bayraktar, A., Türker, T., and Altunişik, A. C.: Experimental frequencies and damping ratios for historical masonry arch bridges, Construction and Building Materials, 75, 234-241, https://doi.org/10.1016/j.conbuildmat.2014.10.044, 2015.

Bottelin, P., Lévy, C., Baillet, L., Jongmans, D., and Guéguen, P.: Modal and thermal analysis of Les Arches unstable rock column (Vercors massif, French Alps), Geophysical Journal International, 194, 849-858, https://doi.org/10.1093/gji/ggt046, 2013.

290   Brincker, R., Zhang, L., and Andersen, P.: Modal identification of output-only systems using frequency domain decomposition, Smart Materials and Structures, 10, 441-445, https://doi.org/10.1088/0964-1726/10/3/303, 2001b.

Brincker, R., and Ventura, C.: Introduction to operational modal analysis, John Wiley & Sons Inc, Chichester, UK, 360 pp., 2015.

Bruthans, J., Soukup, J., Vaculikova, J., Filippi, M., Schweigstillova, J., Mayo, A. L., Masin, D., Kletetschka, G., and Rihosek, J.: Sandstone landforms shaped by negative feedback between stress and erosion, Nature Geoscience, 7, 597-601, 10.1038/ngeo2209, 2014.

295   Burjánek, J., Moore, J. R., Yugsi Molina, F. X., and Fäh, D.: Instrumental evidence of normal mode rock slope vibration, Geophysical Journal International, 188, 559-569, doi:10.1111/j.1365-246X.2011.05272.x, 2012.

Burjánek, J., Gischig, V., Moore, J. R., and Fäh, D.: Ambient vibration characterization and monitoring of a rock slope close to collapse, Geophysical Journal International, 212, 297-310, https://doi.org/10.1093/gji/ggx424, 2018.

300 Cheynet, E., Jakobsen, J. B., and Snæbjörnsson, J.: Damping estimation of large wind-sensitive structures, Procedia Engineering, 199, 2047-2053, https://doi.org/10.1016/j.proeng.2017.09.471, 2017.

Cheynet, E.: Operational modal analysis with automated SSI-COV algorithm, Zenodo, 10.5281/ZENODO.3774061, 2020.

Chopra, A. K.: Dynamics of structures : theory and applications to earthquake engineering, fourth ed., Prentice-Hall international series in civil engineering and engineering mechanics, Boston : Pearson Prentice Hall, 2015.

Cole, H. A.: On-line failure detection and damping measurement of aerospace structures by random decrement signatures, NASA CR, Vol. 305 2205, Washington, Print. NASA CR., 1973.

Colombero, C., Jongmans, D., Fiolleau, S., Valentin, J., Baillet, L., and Bièvre, G.: Seismic Noise Parameters as Indicators of Reversible Modifications in Slope Stability: A Review, Surveys in Geophysics, 42, 339-375, 10.1007/s10712-021-09632-w, 2021.

DeseretNews: Slabs fall from landscape arch: https://www.deseret.com/1991/9/7/18939827/slabs-fall-from-landscape-arch, access: 10.12.2020, 1991.

310 Geimer, P. R., Finnegan, R., and Moore, J. R.: Sparse Ambient Resonance Measurements Reveal Dynamic Properties of Freestanding Rock Arches, Geophysical Research Letters, 47, e2020GL087239, https://doi.org/10.1029/2020GL087239, 2020.

Häusler, M., Michel, C., Burjánek, J., and Fäh, D.: Fracture Network Imaging on Rock Slope Instabilities Using Resonance Mode Analysis, Geophysical Research Letters, 46, 6497-6506, https://doi.org/10.1029/2019GL083201, 2019.

Häusler, M., Michel, C., Burjánek, J., and Fäh, D.: Monitoring the Preonzo rock slope instability using resonance mode analysis, Journal of 315 Geophysical Research: Earth Surface, n/a, e2020JF005709, https://doi.org/10.1029/2020JF005709, 2021.

Iannucci, R., Martino, S., Paciello, A., D'Amico, S., and Galea, P.: Investigation of cliff instability at Għajn Ħadid Tower (Selmun Promontory, Malta) by integrated passive seismic techniques, Journal of Seismology, 24, 897-916, 10.1007/s10950-019-09898-z, 2020.

Kleinbrod, U., Burjánek, J., and Fäh, D.: Ambient vibration classification of unstable rock slopes: A systematic approach, Engineering Geology, 249, 198-217, https://doi.org/10.1016/j.enggeo.2018.12.012, 2019.

320 Lévy, C., Baillet, L., Jongmans, D., Mourot, P., and Hantz, D.: Dynamic response of the Chamousset rock column (Western Alps, France), Journal of Geophysical Research: Earth Surface, 115, https://doi.org/10.1029/2009JF001606, 2010.

Magalhães, F., Cunha, Á., and Caetano, E.: Online automatic identification of the modal parameters of a long span arch bridge, Mechanical Systems and Signal Processing, 23, 316-329, https://doi.org/10.1016/j.ymssp.2008.05.003, 2009.

Mercerat, E. D., Payeur, J. B., Bertrand, E., Malascrabes, M., Pernoud, M., and Chamberland, Y.: Deciphering the dynamics of a 325 heterogeneous sea cliff using ambient vibrations: case study of the Sutta-Rocca overhang (southern Corsica, France), Geophysical Journal International, 224, 813-824, 10.1093/gji/ggaa465, 2021.

Michel, C., Guéguen, P., Lestuzzi, P., and Bard, P. Y.: Comparison between seismic vulnerability models and experimental dynamic properties of existing buildings in France, Bulletin of Earthquake Engineering, 8, 1295-1307, 10.1007/s10518-010-9185-7, 2010.

Moore, J. R., Geimer, P. R., Finnegan, R., and Thorne, M. S.: Use of Seismic Resonance Measurements to Determine the Elastic Modulus 330 of Freestanding Rock Masses, Rock Mechanics and Rock Engineering, 51, 3937-3944, 10.1007/s00603-018-1554-6, 2018.

Moore, J. R., Geimer, P. R., Finnegan, R., and Bodtker, J.: Between a beam and catenary: Influence of geometry on gravitational stresses and stability of natural rock arches, Geomorphology, 364, 107244, https://doi.org/10.1016/j.geomorph.2020.107244, 2020.

Ostanin, I., Safonov, A., and Oseledets, I.: Natural Erosion of Sandstone as Shape Optimisation, Scientific Reports, 7, 17301, 10.1038/s41598-017-17777-1, 2017.

335 Peeters, B., and De Roeck, G.: Reference-based stochastic subspace identification for output-only modal analysis, Mechanical Systems and Signal Processing, 13, 855-878, https://doi.org/10.1006/mssp.1999.1249, 1999.

Poggi, V., Ermert, L., Burjanek, J., Michel, C., and Fäh, D.: Modal analysis of 2-D sedimentary basin from frequency domain decomposition of ambient vibration array recordings, Geophysical Journal International, 200, 615-626, https://doi.org/10.1093/gji/ggu420, 2015.

Preiswerk, L. E., Michel, C., Walter, F., and Fäh, D.: Effects of geometry on the seismic wavefield of Alpine glaciers, Annals of Glaciology, 340 60, 112-124, 10.1017/aog.2018.27, 2019.

Satariano, B., and Gauci, R.: Landform Loss and Its Effect on Health and Well-being: The Collapse of the Azure Window (Gozo) and the Resultant Reactions of the Media and the Maltese Community, in: Landscapes and Landforms of the Maltese Islands, edited by: Gauci, R., and Schembri, J. A., Springer International Publishing, Cham, 289-303, 2019.

Starr, A. M., Moore, J. R., and Thorne, M. S.: Ambient resonance of Mesa Arch, Canyonlands National Park, Utah, Geophysical Research 345 Letters, 42, 6696-6702, https://doi.org/10.1002/2015GL064917, 2015.

van Overschee, P.: Subspace Identification for Linear Systems : Theory — Implementation — Applications, 1st ed. 1996. ed., edited by: de Moor, B. L., Springer US, New York, NY, 1996.

Weber, S., Fäh, D., Beutel, J., Faillettaz, J., Gruber, S., and Vieli, A.: Ambient seismic vibrations in steep bedrock permafrost used to infer variations of ice-fill in fractures, Earth and Planetary Science Letters, 501, 119-127, https://doi.org/10.1016/j.epsl.2018.08.042, 2018.

350 Woodroffe, C. D.: Coasts : form, process and evolution, Cambridge : Cambridge University Press, 2002.